We are IntechOpen, the world's leading publisher of Open Access books Built by scientists, for scientists

6,900
Open access books available

185,000
International authors and editors

200M
Downloads

Our authors are among the

154
Countries delivered to

TOP 1%
most cited scientists

12.2%
Contributors from top 500 universities



WEB OF SCIENCE™

Selection of our books indexed in the Book Citation Index in Web of Science™ Core Collection (BKCI)

Interested in publishing with us?
Contact book.department@intechopen.com

Numbers displayed above are based on latest data collected.
For more information visit www.intechopen.com



Chapter 5

Risk Assessment of NPP Safety in Case of Emergency Situations on Technology

Juraj Králik

Additional information is available at the end of the chapter

http://dx.doi.org/10.5772/intechopen.68772

Abstract

The last accidents of the nuclear power plant (NPP) in Chernobyl and Fukushima give us the new inspiration to verify the safety level of the NPP structures. This paper presents the new requirements to test the safety and reliability of the NPP structures due to the recent accidents in the world. The IAEA in Vienna required in the document 'Stress tests' the verification of the safety of the NPP structures under impact of the extreme loads as the earthquakes, the extreme climatic actions and the technology accidents. The new recommendations to load combinations and design criteria were defined. The risk assessment to verify the safety and reliability of the NPP structures based on probabilistic and nonlinear analysis is presented. The uncertainties of material model (behaviour of the reinforcement and liner, concrete cracking and crushing), degradation effects, the loads level (dead and live loads, extreme climatic and accidental temperature and overpressure) as well as other effects following from the inaccuracy of the calculated model and numerical methods were taken into account in the response surface method (RSM) method. The results of the deterministic and probabilistic analysis of the NPP structures are presented.

Keywords: risk, stress test, accident, safety, probability, nonlinearity, VVER, NPP

1. Introduction

The nuclear technology gives us the perspective of the effective use of natural resources of energy, but on the other hand, it is a risk for the environment [1–4]. The first accident in nuclear research facilities dates back to 21 May 1946. A nuclear critical accident occurred at the Los Alamos Scientific Laboratory in New Mexico. Severe problems arrived after an accident in Chernobyl Nuclear Power Plant in Ukraine on 26 April 1986. The last massive nuclear power plant (NPP) accident was on 11 March 2011 in Fukushima [5–7]. Following a major earthquake

INTECH
open science | open minds

© 2017 The Author(s). Licensee InTech. This chapter is distributed under the terms of the Creative Commons Attribution License (http://creativecommons.org/licenses/by/3.0), which permits unrestricted use, distribution, and reproduction in any medium, provided the original work is properly cited. CC BY

(a magnitude 7.1), a 15-m tsunami disabled the power supply and cooling of three Fukushima Daiichi reactors, hence causing a nuclear accident.

In view of the analysis results of the Fukushima accident [5, 6], the owner and operator of nuclear power plants (NPPs) in Slovakia re-evaluated the safety and reliability of structures and technology of all objects, according to the recommendations in "Stress tests" on all units in operation or under construction [7]. The main plant technological equipment (except for main circulation pumps) for all units was manufactured either in Czech Republic or in Slovakia [3].

In the process of design, construction and operation of plants, significant improvements in safety were made compared to the original project, including enhanced resistance to external hazards [1–3, 8]. Lately, in addition to previous safety improvements, many proposals have been implemented in the reconstruction process of NPP structures with reactor VVER 440/V213 in Slovakia for mitigation of severe accidents [3]. Fifty-one per cent of the overall production of electricity in SR comes from the nuclear power plants (**Table 1**).

The NPP buildings with the reactor VVER 440/213 consist of the turbine hall, middle building, reactor building and bubble condenser [1]. The NPP containment is limited by the area of reactor building and bubble tower (**Figure 1**). In the case of the loss-of-coolant accident (LOCA), the

Source	2007	%	2008	%	2009	%
Nuclear power plants	15,335	51.80	16,704	56.00	14,081	51.42
Thermal power plants	5421	18.30	5647	18.93	4768	17.41
Hydroelectric power plants	4485	15.10	4284	14.36	4662	17.02
Other power plants	2666	9.00	2674	8.96	2563	9.36
Import saldo	1725	5.80	521	1.75	1312	4.79
Consumption SR	29,632	100.00	29,830	100.00	27,386	100.00
Production SR	27,907		29,309		26,074	

Table 1. Source ratio on annual electricity consumption in SR.

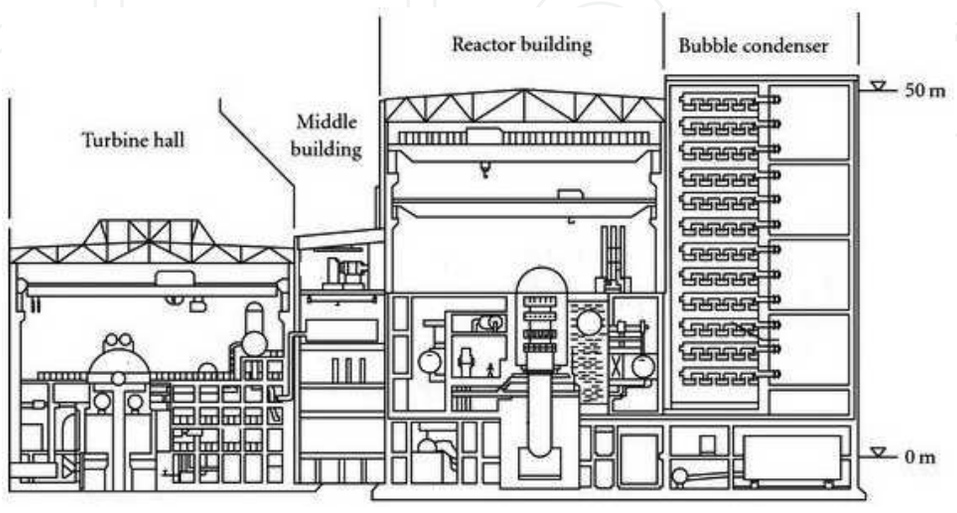


Figure 1. Section plane of the containment with reactor VVER440/213.

steam expands in the containment space, and the overpressure and temperature loads affect the containment structure [1]. The structural integrity and the tightness of the containment must be guaranteed in the case of the technology accident.

2. Safety assessment of the NPP risk

The International Atomic Energy Agency (IAEA) set up a programme [8] to give guidance to its member states on the many aspects of the safety of nuclear power reactors. The IAEA standards [8–10] and the US Nuclear Regulatory Commission (NRC) [4, 11] define the principal steps for the calculation of the risk of the NPP performance by simulations using Latin hypercube sampling (LHS) probabilistic method as follows:

1. Accident frequency (systems) analysis
2. Accident progression analysis
3. Radioactive material transport (source-term) analysis
4. Offsite consequence analysis
5. Risk integration.

The final stage of the probabilistic safety analysis (PSA) is the compilation of the outputs of the first four steps into an expression of risk. The risk integration is shown in matrix formulation in **Figure 2**. The approximate numbers of plant damage states (PDSs), accident progression bins (APBs), and source-term groups (STGs), and the number of consequences are presented in the different reports [1–3, 12] and standards [4, 10–13].

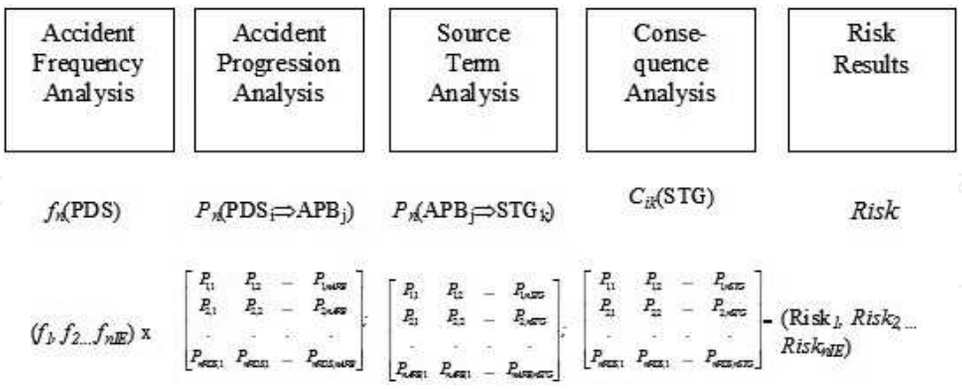


Figure 2. Scheme of Latin hypercube sampling.

3. Safety of the NPP structure resistance

In the case of the loss-of-coolant accident (LOCA) [3, 17, 18], the steam pressure expands from the reactor hall to the bubble condenser. Hence, the reactor hall and the bubble condenser are the critical structures of the NPP hermetic zone.

In the past, the calculation of the structural reliability for containment of the type of VVER 440/213 was carried out determining the probability density function for the ultimate pressure. A basis for the calculations consisted in results of linear and non-linear analysis, depending on whether the modelling considered the update of the properties.

The present work analyses the impact of combination of pressure load with thermal load that can arise in extreme situations related to severe accident progression. To achieve proper results, a detailed finite-element analysis of the concrete structure was carried out using ANSYS software and the programs CRACK [3, 14–18] were employed to solve this task. The basis for the probabilistic evaluation is reviewed, considering the uncertainties connected with loads and material properties. In the "Result" section, a comparison with linear evaluation is also mentioned.

3.1. Scenario of the hard accident

Most of the countries rate the safety of the NPP hermetic structures through the double-ended break guillotine test of the largest pipe in the reactor coolant system. During the design process of NPP structures with reactors VVER-440/230 type, the guillotine break of 2 × 500-mm pipes was considered as a beyond-design-basis accident (BDBA). The scenario of the hard accident is based on the assumption of the extreme situation where a loss of primary coolant accident (LOCA) is combined with the total loss of containment cooling system. During this situation, the hermetic zone cannot be available due to the external spraying of borated water. In practice, the contribution to heating from hydrogen explosion shall also be accounted.

In addition, the extremely climatic temperature (negative or positive) impacts the external slabs and walls of the hermetic zone. The temperature boundary conditions are defined to comply with the new revision of reference temperature provided by the Slovak hydro-meteorological institute (SHMU) [3] and relevant Eurocodes [22] for a return period of 10^4 year. Three types of the scenarios were considered (**Table 2**).

3.2. Steel and concrete material properties under high-temperature impact

The recapitulation of the research works and the standard recommendations for the steel and concrete under high-temperature effect are summarized in US NRC report [23] and Eurocodes [22].

Type	Duration	Over-pressure [kPa]	Extreme temperatures [°C]		
			Interior	Exterior	
				Max.	Min.
I.	1 day	150	127	42	−28
II.	7 days	250	150	42	−28
III.	1 year	–	80–120	42	−28

Table 2. The scenarios of the accidents in the hermetic zone.

The recommendations for the design of the structures are described in the US standards ACI [24], CEB-FIP Model Code [25] and Eurocodes [22]. The bonding phases of concrete are from the instable substance, which can be destructed at high temperature and their microstructures are changed.

The thermal conductivity λ_c of normal weight concrete may be determined between the lower and upper limits given hereafter. The upper limit has been derived from tests of steel-concrete composite structural elements. The CEB-FIP Model Code [25] and Eurocodes [22] define the stress-strain relationship for concrete and steel materials dependent on temperature θ for heating rates between 2 and 50 K/min. In the case of the concrete, the stress–strain diagram is divided into two regions. The concrete strength $\sigma_{c,\theta}$ increases in the first region and decreases in the second region (**Figure 3**).

The stress-strain relations $\sigma_{c,\theta} \approx \varepsilon_{c,\theta}$ in region I are defined in the following form:

$$\sigma_{c,\theta} = f_{c,\theta}\left[3\left(\frac{\varepsilon_{c,\theta}}{\varepsilon_{cu,\theta}}\right) \Big/ \left\{2 + \left(\frac{\varepsilon_{c,\theta}}{\varepsilon_{cu,\theta}}\right)^3\right\}\right], \qquad f_{c,\theta} = k_{c,\theta} f_c, \tag{1}$$

where the strain $\varepsilon_{cu,\theta}$ corresponds to stress $f_{c,\theta}$, the reduction factor can be chosen according to standard [22]. The reduction factors $k_{c,\theta}$ ($k_{c,\theta}$ = 0.925 for θ_c = 150°C) for the stress–strain relationship are considered in accordance with the standard.

The stress-strain relationships for steel (**Figure 4**) are considered in accordance with Eurocode [22] on dependency of temperature level for heating rates between 2 and 50 K/min. In the case of steel, the stress-strain diagram is divided into four regions.

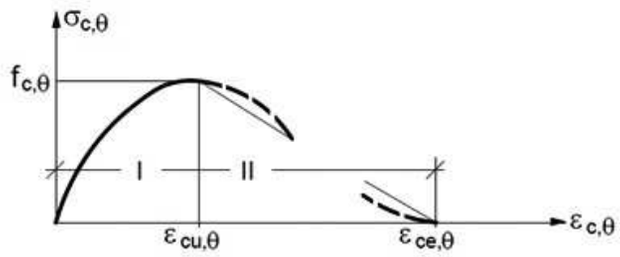


Figure 3. Stress-strain relationship of the concrete dependent on temperature [22].

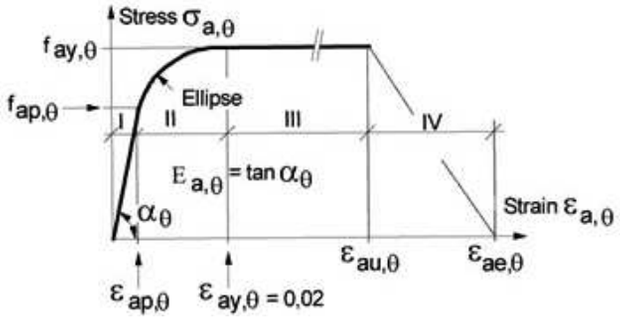


Figure 4. Stress-strain relationship of the steel dependent on temperature [22].

The stress–strain relations $\sigma_{a,\theta} \approx \varepsilon_{a,\theta}$ are defined in the following form in region I:

$$\sigma_{a,\theta} = E_{a,\theta}\varepsilon_{a,\theta}, \quad E_{a,\theta} = k_{E,\theta}E_a \tag{2}$$

where the reduction factor $k_{E,\theta}$ can be chosen according to the values of [10].

In region II:

$$\begin{aligned} &\sigma_{a,\theta} = (f_{ay} - c) + \frac{b}{a}\sqrt{a^2 - (\varepsilon_{ay,\theta} - \varepsilon_{a,\theta})^2}, a^2 = (\varepsilon_{ay,\theta} - \varepsilon_{ap,\theta})(\varepsilon_{ay,\theta} - \varepsilon_{ap,\theta} + c/E_{a,\theta}), \\ &b^2 = E_{a,\theta}(\varepsilon_{ay,\theta} - \varepsilon_{ap,\theta})c + c^2, c = \frac{(f_{ay,\theta} - f_{ap,\theta})^2}{E_{a,\theta}(\varepsilon_{ay,\theta} - \varepsilon_{ap,\theta}) - 2(f_{ay,\theta} - f_{ap,\theta})} \end{aligned} \tag{3}$$

and in region III:

$$\sigma_{a,\theta} = f_{ay,\theta} \tag{4}$$

A graphical display of the stress-strain relationships for steel grade S235 is presented in **Figure 4** up to the maximum strain of $\varepsilon_{ay,\theta} = 2\%$.

The strength and deformation properties of reinforcing steels under elevating temperatures may be obtained by the same mathematical model as that presented for structural steel S235. The reduction factors $k_{E,\theta}$($k_{E,\theta}$ = 0.95 for θ_a = 150°C) for the stress-strain relationship are considered in accordance with the standard.

The material properties of the concrete structures in the numerical model were considered using the experimental tests statistically evaluated during the performance of the nuclear power plant [3, 28]. The material properties of the steel structures were not changed during plant performance [3].

3.3. Nonlinear model of steel and reinforced concrete structures

The theory of large strain and rate-independent plasticity was proposed during the high-overpressure loading using the SHELL181-layered shell element from (**Figure 5**) the ANSYS library [26].

The vector of the displacement of the lth-shell layer $\{u^l\} = \{u^l_{x'}, u^l_{y'}, u^l_z\}^T$ is approximated by the quadratic polynomial [26] in the form

$$\{u^l\} = \begin{Bmatrix} u^l_x \\ u^l_y \\ u^l_z \end{Bmatrix} = \sum_{i=1}^{4} N_i . \begin{Bmatrix} u_{xi} \\ u_{yi} \\ u_{zi} \end{Bmatrix} + \sum_{i=1}^{4} N_i . \frac{\zeta . t_i}{2} . \begin{bmatrix} a_{1,i} & b_{1,i} \\ a_{2,i} & b_{2,i} \\ a_{3,i} & b_{3,i} \end{bmatrix} . \begin{Bmatrix} \theta_{xi} \\ \theta_{yi} \end{Bmatrix} \tag{5}$$

where N_i is the shape function for i-node of the 4-node shell element, u_{xi}, u_{yi}, and u_{zi} are the motions of i-node, ζ is the thickness coordinate, t_i is the thickness at i-node, $\{a\}$ is the unit vector in x-direction, $\{b\}$ is the unit vector in the plane of element and normal to $\{a\}$, θ_{xi} or θ_{yi} are the rotations of i-node about vector $\{a\}$ or $\{b\}$.

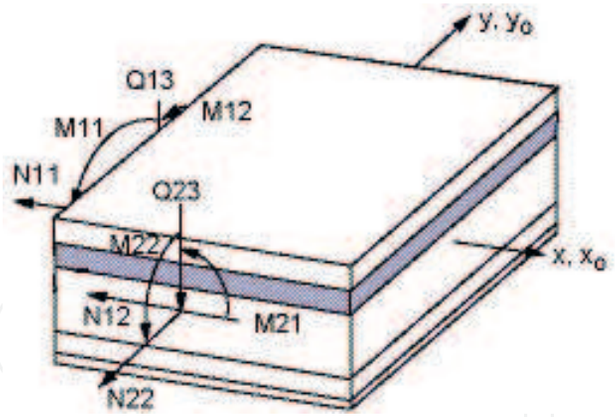


Figure 5. SHELL181-layered element with smeared reinforcements [26].

In the case of the elastic state, the stress–strain relations for the *l*th-layer are defined in the form

$$\{\sigma^l\} = [D_e^l]\{\varepsilon^l\} \tag{6}$$

where strain and stress vectors are as follows: $\{\varepsilon^l\}^T = \{\varepsilon_x, \varepsilon_y, \gamma_{xy}, \gamma_{yz}, \gamma_{zx}\}$, $\{\sigma^l\}^T = \{\sigma_x, \sigma_y, \tau_{xy}, \tau_{yz}, \tau_{zx}\}$ and the matrix of the material stiffness.

3.3.1. Geometric nonlinearity

If the rotations are large while the mechanical strains (those that cause stresses) are small, then it is possible to use a large rotation procedure. A large rotation analysis is performed in a static analysis in the ANSYS program [26].

From the following relations, the strain in the *n*-step of the solution can be computed:

$$\{\varepsilon_n\} = [B_o][T_n]\{u_n\} \tag{7}$$

Where $\{u_n\}$ is the displacement vector, $[B_o]$ is the original strain–displacement relationship and $[T_n]$ is the orthogonal transformation relating the original element coordinates to the convected (or rotated) element coordinates.

3.3.2. Material nonlinearity

The technology segments on board of the hermetic zone are made from the steel. The finite element model (FEM) of these segments is based on the HMH-yield criterion for the isotropic and homogenous material properties.

Consequently the stress–strain relations are obtained from the following relations

$$\{d\sigma\} = [D_{el}](\{d\varepsilon\} - \{d\varepsilon^{pl}\}) = [D_{el}]\left(\{d\varepsilon\} - d\lambda\left\{\frac{\partial Q}{\partial \sigma}\right\}\right) = [D_{ep}]\{d\varepsilon\} \tag{8}$$

where $[D_{ep}]$ is elastic-plastic matrix in the form

$$\left[D_{ep}\right] = [D_e] - \frac{[D_e]\left\{\frac{\partial Q}{\partial \sigma}\right\}\left\{\frac{\partial F}{\partial \sigma}\right\}^T[D_e]}{A + \left\{\frac{\partial F}{\partial \sigma}\right\}^T[D_e]\left\{\frac{\partial Q}{\partial \sigma}\right\}} \tag{9}$$

The hardening parameter A depends on the yield function and model of hardening (isotropic or kinematic). Huber-Mises-Hencky (HMH) yield is defined in the form

$$\sigma_{eq} = \sigma_T(\kappa), \tag{10}$$

Where σ_{eq} is the equivalent stress in the point and $\sigma_o(\kappa)$ is the yield stress that depends on the hardening.

In the case of kinematic hardening by Prager (vs Ziegler) and the ideal Bauschinger's effect, it is given as

$$A = \frac{2}{9E}\sigma_T^2 H' \tag{11}$$

The hardening modulus H' for this material is defined in the form

$$H' = \frac{d\sigma_{eq}}{d\varepsilon_{eq}^p} = \frac{d\sigma_T}{d\varepsilon_{eq}^p} \tag{12}$$

When this criterion is used with the isotropic hardening option, the yield function is given by

$$F(\sigma) = \sqrt{\{\sigma\}^T[M]\{\sigma\}} - \sigma_o(\varepsilon_{ep}) = 0 \tag{13}$$

where $\sigma_o(\varepsilon_{ep})$ is the reference yield stress, ε_{ep} is the equivalent plastic strain and the matrix [M] is as follows:

$$[M] = \begin{bmatrix} 1 & 0 & 0 & 0 & 0 & 0 \\ 0 & 1 & 0 & 0 & 0 & 0 \\ 0 & 0 & 1 & 0 & 0 & 0 \\ 0 & 0 & 0 & 2 & 0 & 0 \\ 0 & 0 & 0 & 0 & 2 & 0 \\ 0 & 0 & 0 & 0 & 0 & 2 \end{bmatrix} \tag{14}$$

3.3.3. Nonlinear material model of the concrete structures

The presented constitutive model is a further extension of the smeared and oriented crack model, which was developed in [3]. A new concrete cracking-layered finite shell element was developed and incorporated into the ANSYS system [3] considering the experimental tests of real reinforced concrete plate and wall structures. The layered shell elements are proposed considering the nonlinear properties of the concrete and steel depending on temperature.

The concrete compressive stress f_c, the concrete tensile stress f_t and the shear modulus G are reduced during the crushing or cracking of the concrete. These effects are updated on the numerical model.

http://dx.doi.org/10.5772/intechopen.68772

In this model, the stress-strain relation is defined (**Figure 6**) following CEB-FIP Model Code [25]:

- Loading-compression region $\varepsilon_{cu} < \varepsilon^{eq} < 0$

$$\sigma_c^{ef} = f_c^{ef}.\frac{k.\eta - \eta^2}{1 + (k-2).\eta}, \eta = \frac{\varepsilon^{eq}}{\varepsilon_c}, (\varepsilon_c \doteq -0.0022, \varepsilon_{cu} \doteq -0.0035) \tag{15}$$

- Softening-compression region $\varepsilon_{cm} < \varepsilon^{eq} < \varepsilon_{cu}$

$$\sigma_c^{ef} = f_c^{ef}.\left(1 - \frac{\varepsilon^{eq} - \varepsilon_c}{\varepsilon_{cm} - \varepsilon_{cu}}\right) \tag{16}$$

- The tension region $\varepsilon_t < \varepsilon^{eq} < \varepsilon_m$

$$\sigma_c^{ef} = f_t.\exp\left(-2.(\varepsilon^{eq} - \varepsilon_t)/\varepsilon_{tm}\right), (\varepsilon_t \doteq 0.0001, \varepsilon_{tm} \doteq 0.002) \tag{17}$$

The equivalent values of f_t^{eq} and f_c^{eq} were considered for the plane stress state. The relation between the one and bidimensional stresses state was considered in the plane of principal stresses (σ_{c1}, σ_{c2}) of each shell layer by Kupfer (see **Figure 7**) [3].

The shear concrete modulus G was defined for cracking concrete by Kolmar [23] in the form

$$G = r_g.G_o, r_g = \frac{1}{c_2}\ln\left(\frac{\varepsilon_u}{c_1}\right), c_1 = 7 + 333(p - 0.005), c_2 = 10 - 167(p - 0.005) \tag{18}$$

where G_o is the initial shear modulus of concrete, ε_u is the strain in the normal direction to crack, c_1 and c_2 are the constants dependent on the ratio of reinforcing and p is the ratio of reinforcing transformed to the plane of the crack ($0 < p < 0.02$).

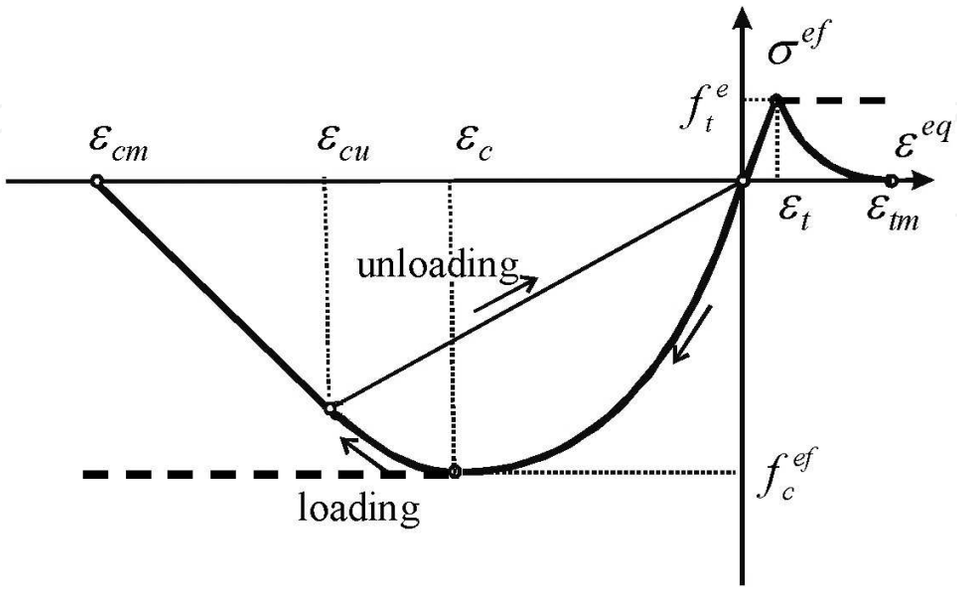


Figure 6. The concrete stress-strain diagram.

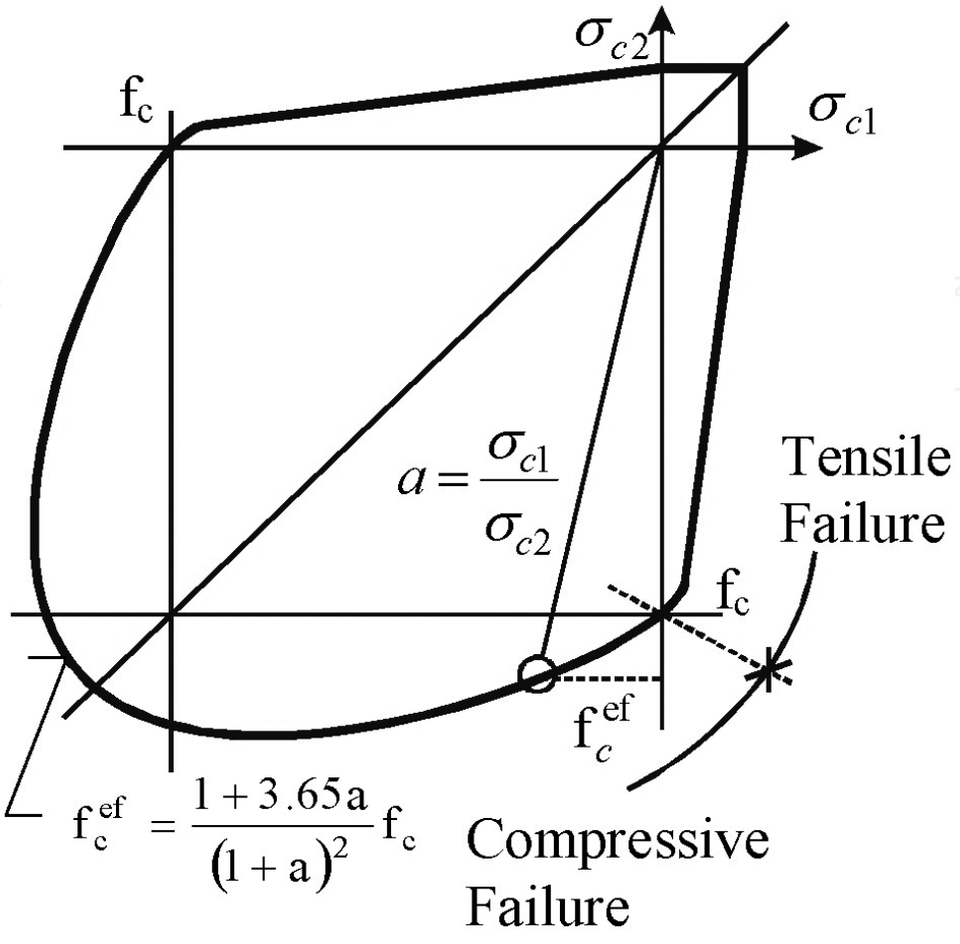


Figure 7. Kupfer's plasticity function.

The strain-stress relationship in the Cartesian coordinates can be defined in dependency on the direction of the crack (in the direction of principal stress, vs strain)

$$[\sigma_{cr}] = [D_{cr}]\{\varepsilon_{cr}\} \text{ and } [\sigma] = [T_\sigma]^{\mathrm{T}}[D_{cr}][T_\varepsilon]\{\varepsilon\} \tag{19}$$

$$[D_{cr}^l] = [T_{c.\sigma}^l]^{\mathrm{T}}[D_{cr}^l][T_{c.\varepsilon}^l] + \sum_{s=1}^{N_{rein}} [T_s^l]^{\mathrm{T}}[D_s^l][T_s^l] \tag{20}$$

where $[T_{c.\sigma}]$, $[T_{c.\varepsilon}]$ and $[T_s]$ are the transformation matrices for the concrete and the reinforcement separately, N_{rein} is the number of the reinforcements in the lth–layer (**Figure 8**).

The stress-strain relationship for the concrete lth-layer cracked in one direction is

$$\begin{Bmatrix} \sigma_1 \\ \sigma_2 \\ \tau_{12} \\ \tau_{13} \\ \tau_{23} \end{Bmatrix}_l = \begin{bmatrix} 0 & 0 & 0 & 0 & 0 \\ 0 & E & 0 & 0 & 0 \\ 0 & 0 & G_{12}^{cr} & 0 & 0 \\ 0 & 0 & 0 & G_{13}^{cr} & 0 \\ 0 & 0 & 0 & 0 & G_{23}^{cr} \end{bmatrix}_l \begin{Bmatrix} \varepsilon_1 \\ \varepsilon_2 \\ \gamma_{12} \\ \gamma_{13} \\ \gamma_{23} \end{Bmatrix}_l \tag{21}$$

http://dx.doi.org/10.5772/intechopen.68772

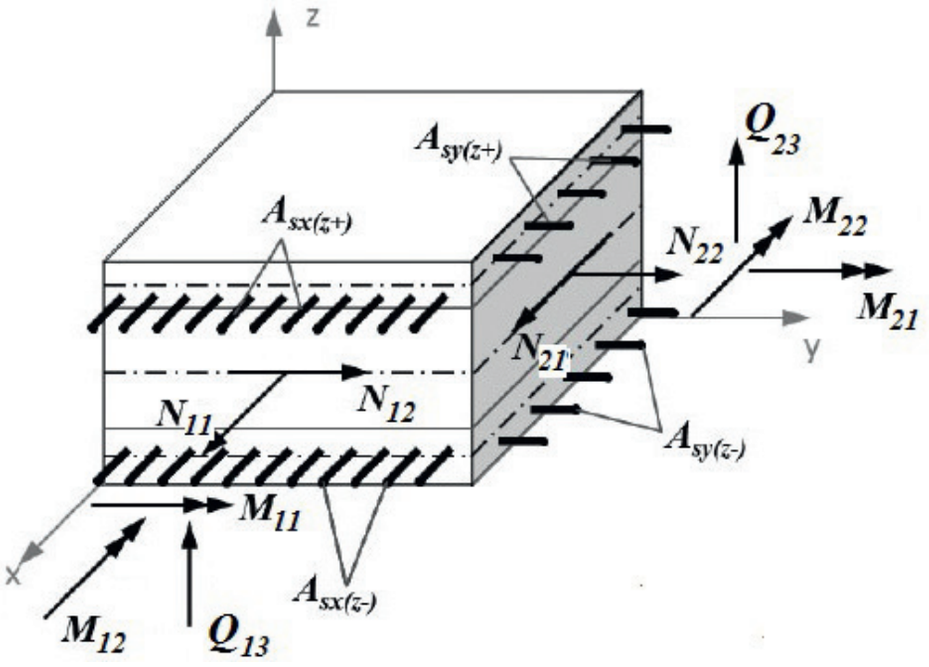


Figure 8. SHELL181-layered element with smeared reinforcements.

When the tensile stress in the 2-directions reaches the value f'_t, the latter cracked plane perpendicular to the first one is assumed to be formed, and the stress–strain relationship becomes

$$\begin{Bmatrix} \sigma_1 \\ \sigma_2 \\ \tau_{12} \\ \tau_{13} \\ \tau_{23} \end{Bmatrix}_l = \begin{bmatrix} 0 & 0 & 0 & 0 & 0 \\ 0 & 0 & 0 & 0 & 0 \\ 0 & 0 & G_{12}^{cr}/2 & 0 & 0 \\ 0 & 0 & 0 & G_{13}^{cr} & 0 \\ 0 & 0 & 0 & 0 & G_{23}^{cr} \end{bmatrix}_l \begin{Bmatrix} \varepsilon_1 \\ \varepsilon_2 \\ \gamma_{12} \\ \gamma_{13} \\ \gamma_{23} \end{Bmatrix}_l \tag{22}$$

where the shear moduli are reduced by parameters r_{g1} and r_{g2} by Kolmar [27] as follows:

$$G_{12}^{cr} = G_o.r_{g1}, G_{13}^{cr} = G_o.r_{g1}, G_{23}^{cr} = G_o r_{g2}.$$

The stress-strain relationship defined in the direction of the principal stresses must be transformed to the reference axes XY. The simplified smeared model of the concrete cracked is more convenient for finite element formulation than the singular discrete model.

The smeared calculation model is determined by the size of the finite element, hence its characteristic dimension $L_c = \sqrt{A}$, where A is the element area (vs integrated point area of the element). The assumption of constant failure energies G_f = const is proposed in the form

$$G_f = \int_0^\infty \sigma_n(w)dw = A_G.L_c, \quad w_c = e_w.L_c \tag{23}$$

where w_c is the width of the failure, σ_n is the stress in the concrete in the normal direction and A_G is the area under the stress-strain diagram of concrete in tension. The descend line of

concrete stress-strain diagram can be defined on dependency on the failure energies [25] by the modulus in the form

$$E_{c,s} = E_c/(1-\lambda_c), \qquad \lambda_c = 2G_f E_c/(L_c.\sigma_{\max}^2) \tag{24}$$

where E_c is the initial concrete modulus elasticity, $\sigma_{\max}$ is the maximal stress in the concrete tension. From the condition of the real solution of relation (18), it follows that the characteristic dimension of element must satisfy the following condition:

$$L_c \le 2G_f E_c/\sigma_{\max}^2 \tag{25}$$

The characteristic dimension of the element is determined by the size of the failure energy of the element. The theory of a concrete failure was implied and applied to the two-dimensional (2D)-layered shell elements SHELL181 in the ANSYS element library [26]. The CEB-FIP Model Code [25] defines the failure energies G_f [N/mm] depending on the concrete grades and the aggregate size d_a as follows:

$$G_f = (0.0469d_a^2 - 0.5d_a + 26)(f_c/10)^{0,7} \tag{26}$$

The limit of damage at a point is controlled by the values of the so-called crushing or total failure function F_u. The modified Kupfer's condition for the lth-layer of section is as follows:

$$F_u^l = F_u^l(I_{\varepsilon 1}; I_{\varepsilon 2}; \varepsilon_u) = 0, \quad F_u^l = \sqrt{\beta(3J_{\varepsilon 2} + \alpha I_{\varepsilon 1})} - \varepsilon_u = 0\,, \tag{27}$$

where $I_{\varepsilon 1}$, $I_{\varepsilon 2}$ are the strain invariants, and ε_u is the ultimate total strain extrapolated from uniaxial test results (ε_u = 0.002 in the tension domain, or ε_u = 0.0035 in the compression domain), and α, β are the material parameters determined from Kupfer's experiment results (β = 1.355, α = 1.355ε_u).

The failure function of the whole section will be obtained by the integration of the failure function through the whole section in the form

$$F_u = \frac{1}{t}.\int_0^t F_u^l(I_{\varepsilon 1}; I_{\varepsilon 2}; \varepsilon_u)\, dz = \frac{1}{t}\sum_{l=1}^{N_{lay}} F_u^l(I_{\varepsilon 1}; I_{\varepsilon 2}; \varepsilon_u) t_l \tag{28}$$

where t_l is the thickness of the lth-shell layer, t is the total shell thickness and N_{lay} is the number of layers.

The maximum strain ε_s of the reinforcement steel in the tension area ($\max(\varepsilon_s) \le \varepsilon_{sm} = 0.01$) and by the maximum concrete crack width w_c ($\max(w_c) \le w_{cm} = 0.3$ mm) determine the local collapse of reinforced concrete structure.

The program CRACK based on the presented nonlinear theory of the layered reinforced concrete shell was adopted in the software ANSYS [3]. These procedures were tested in comparison with the experimental results [3, 15, 17, 28].

http://dx.doi.org/10.5772/intechopen.68772

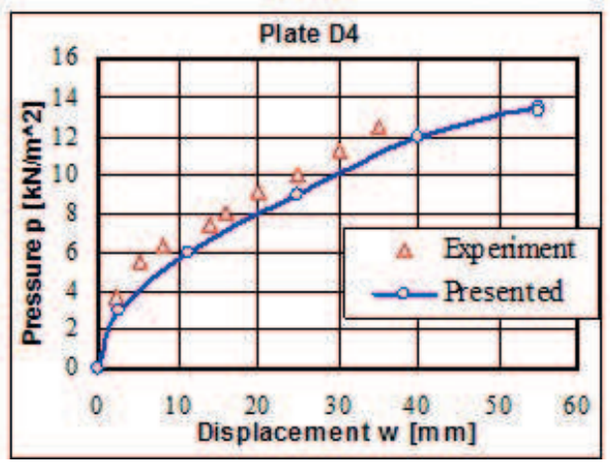


Figure 9. Comparison of experimental and nonlinear numerical analysis of plates.

The reinforced concrete plates D4 (**Figure 9**) with the dimensions 3590/1190/120 mm were simply supported and loaded by pressure p on the area of plate. The plate D4 was reinforced by steel grid KARI Ø8 mm, a′ 150 × 150 mm at the bottom. Material characteristics of plate D4 are the following: Concrete, E_c = 30.9 Gpa, μ = 0.2, f_c = −34.48 Mpa, f_t = 4.5 Mpa and the Reinforcement, E_s = 210.7 Gpa, μ = 0.3, f_s = 550.3 Mpa.

4. Probabilistic assessment

Recent advances and the general accessibility of information technologies and computing techniques give rise to assumptions concerning the wider use of the probabilistic assessment of the reliability of structures through the use of simulation methods in the world [3, 14–22, 29–40]. The probabilistic definition of the reliability condition is of the form

$$g(R,E) = R - E \geq 0 \tag{29}$$

where $g(R,E)$ is the reliability function.

In the case of simulation methods, the failure probability is defined as the best estimation on the base of numerical simulations in the form

$$p_f = \frac{1}{N}\sum_{i=1}^{N} I[g(X_i) \leq 0] \tag{30}$$

where N in the number of simulations, $g(.)$ is the failure function and $I[.]$ is the function with value 1, if the condition in the square bracket is fulfilled, otherwise is equal to 0. The semi- or full-probabilistic methods can be used for the estimation of the structure failure in the critical structural areas. In the case of the semi-probabilistic method, the probabilistic simulation in the critical areas is based on the results of the nonlinear analysis of the full FEM model for the

median values of the input data. The full probabilistic method result from the nonlinear analysis of the series simulated cases considered the uncertainties of the input data.

4.1. Uncertainties of the input data

The action effect E and the resistance R are calculated considering the uncertainties of the input data as follows [3]:

$$E = G_k g_{\text{var}} + Q_k q_{\text{var}} + P_k p_{\text{var}} + T_k t_{\text{var}} \quad \text{and} \quad R = R_k r_{\text{var}} \tag{31}$$

The uncertainties of the input data were taken in accordance with the standard requirements [29, 30–32] (**Table 3**).

4.2. Probabilistic simulation methods

Various simulation methods (direct, modified or approximation methods) can be used for the consideration of the influences of the uncertainty of the input data.

In the case of the nonlinear analysis of the full FEM model, the approximation method RSM (response surface method) is the most effective method [3].

The RSM method is based on the assumption that it is possible to define the dependency between the variable input and the output data through the approximation functions in the following form:

$$Y = c_o + \sum_{i=1}^{N} c_i X_i + \sum_{i=1}^{N} c_{ii} X_i^2 + \sum_{i=1}^{N-1} \sum_{j>i}^{N} c_{ij} X_i X_j \tag{32}$$

where c_o is the constant member; c_i are the constants of the linear member and c_{ij} for the quadratic member, which are given for predetermined schemes for the optimal distribution of the variables or for using the regression analysis after calculating the response. The 'Central

	Quantities		**Histograms**		
Input data	**Charact. value**	**Variable value**	**Type**	**Mean**	**Deviation**
				μ	σ [%]
Dead load	G_k	g_{var}	*N*	1	10
Live load	Q_k	q_{var}	*Beta*	0.643	22.6
Pressure	P_k	p_{var}	*N*	1	8
Temperature	T_k	t_{var}	*Beta*	0.933	14.1
Model	E_k	e_{var}	*N*	1	5
Resistance	R_k	r_{var}	*N*	1	5

Table 3. The variability of input parameters.

Composite Design Sampling' (CCD) method or the 'Box-Behnken Matrix Sampling' (BBM) method [3] can be used to determine the polynomial coefficients.

The philosophy of the RSM method is presented in **Figure 10**. The original system of the global surface is discretized using approximation function. The design of the experiment determines the polynomic coefficients. The efficiency of computation of the experimental design depends on the number of design points. With the increase of the number of random variables, this design approach becomes inefficient. The central composite design, developed by Box and Wilson, is more efficient.

The central CCD method is defined as follows (**Figure 10**):

1. Factorial portion of design—a complete $2k$ factorial design (equals −1, +1).
2. Centre point—no centre points, no ≥1 (generally no = 1).
3. Axial portion of design—two points on the axis of each design variable at distance α from the design centre.

The total number of design points is equal to $N = 2^k + 2k + n_o$. The sensitivity of the variables is determined by the correlation matrices. The RSM method generates the explicit performance function for the implicit or complicated limit-state function. This method is very effective to solve robust and complicated tasks.

4.3. Evaluation of the fragility curve

The PSA approach to the evaluation of probabilistic pressure capacity involves limit-state analyses. The limit states should represent possible failure modes of the confinement functions. The identification of potential failure modes is the first step of a probabilistic containment overpressure evaluation. For each failure mode, the median values were established based on the used failure criteria dependent on the applied loading consisting of temperature, pressure and dead load. Along with the pressure capacities for the leak-type failure modes, leak areas are to be estimated in a probabilistic manner. The expected leak areas are failure mode dependent. After calculation of the fragility or conditional probability of failure of containment at different locations, we must consider a combination of pressure-induced failure probabilities of different break or leak locations within containment.

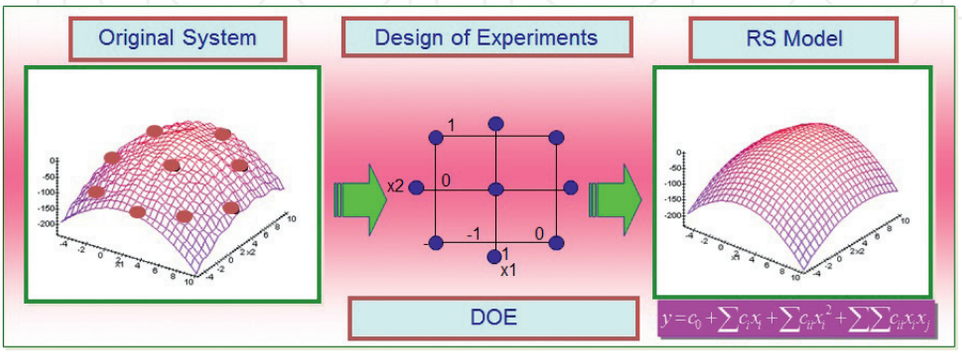


Figure 10. Scheme of the RSM approximation method with the CCD design experiment.

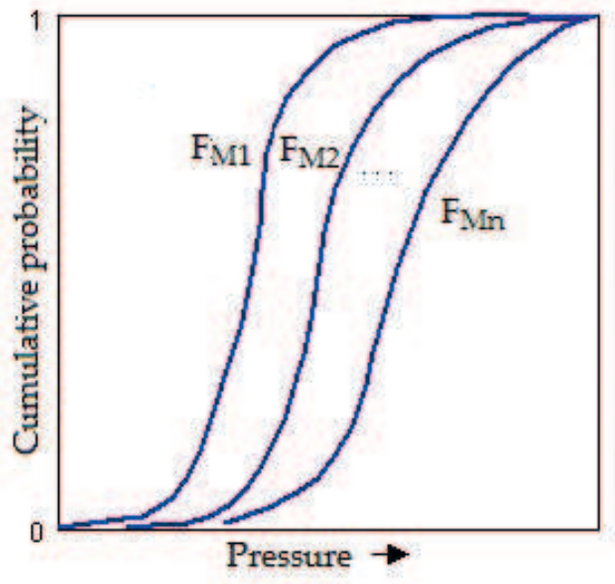


Figure 11. Family of fragility curves showing modelling uncertainty.

Containment may fail at different locations under different failure modes (see **Figure 11**). Consider two failure modes A and B, each with n fragility curves and respective probabilities p_i ($i = 1, \ldots, n$) and q_j ($j = 1, \ldots, n$). Then, the union $C = A \cup B$, the fragility $F_{Cij}(x)$ is given by

$$F_{Cij}(x) = F_{Ai}(x) + F_{Bj}(x) - F_{Ai}(x) \cap F_{Bj}(x) \tag{33}$$

where the subscripts i and j indicate one of the n fragility curves for the failure modes and x denotes a specific value of the pressure within the containment. The probability p_{ij} associated with fragility curve $F_{Cij}(x)$ is given by $p_i.\ q_j$ if the median capacities of the failure modes are independent. The result of the intersection term in Eq. (32) is $F_{Aj}(x).F_{Bj}(x)$ when the randomness in the failure mode capacities is independent and min $[F_{Ai}(x),\ F_{Bj}(x)]$ when the failure modes are perfectly dependent.

The flow is the consequence of an accident that depends on the total leak area. Multiple leaks at different locations of the containment (e.g. bellows, hatch and airlock) may contribute to the total leak area. Using the methodology described earlier, we can obtain the fragility curves for leak at each location.

For a given accident sequence, the induced accident pressure probability distribution, $h(x)$, is known. This is convolved with the fragility curve for each leak location to obtain the probability of leak from that location (P_{Li}). It is understood that there is no break or containment rupture at this pressure.

$$p_{Li} = \int_0^\infty h(x)[1 - F_b(x)]F_l(x)dx \tag{34}$$

Here, the $F_b(x)$ is the fragility of break at the location and $F_l(x)$ is the fragility of the leak. The leak is for each location specified as a random variable with a probability distribution.

5. Probabilistic analysis of the concrete containment

The NPP buildings with the reactor VVER 440/213 consist of the turbine hall, middle building, reactor building and bubble condenser [3]. The building of the power block was idealized with a FEM model consisting of 28 068 elements with 104 287 DOF (**Figures 12** and **13**).

The roof plate of the bubbler tower was defined as the critical area of the containment failure. The probability of the containment failure was determined for various levels of the overpressures Δp = 250, 300, 350, 400, 450 kPa. The probability of the failure was determined by Eqs. (21) and (22) for 10^6 Monte Carlo simulations in program FReET [32].

5.1. Nonlinear deterministic analysis

On the basis of the nonlinear analysis due to the monotone increasing of overpressure inside the hermetic zone, the critical sections of the structure were determined [3]. The resistance of these critical sections was analysed taking into account the design values of the material characteristics and the load. The slab at the top of the bubbler tower building was defined as

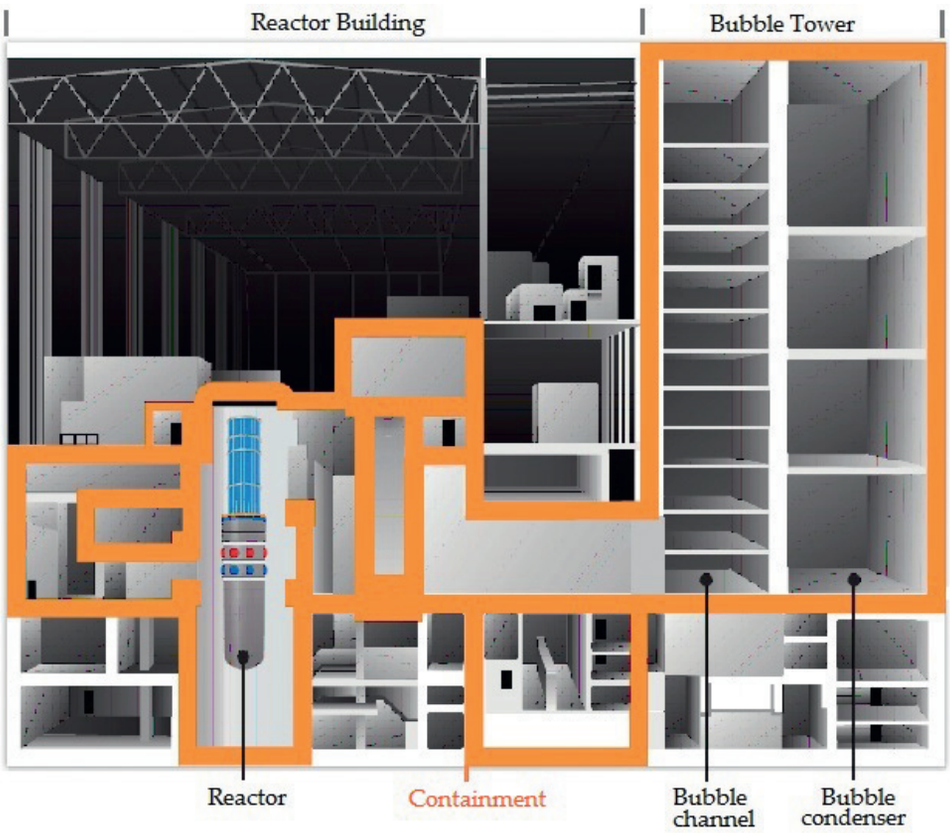


Figure 12. Section plane of the condenser containment.

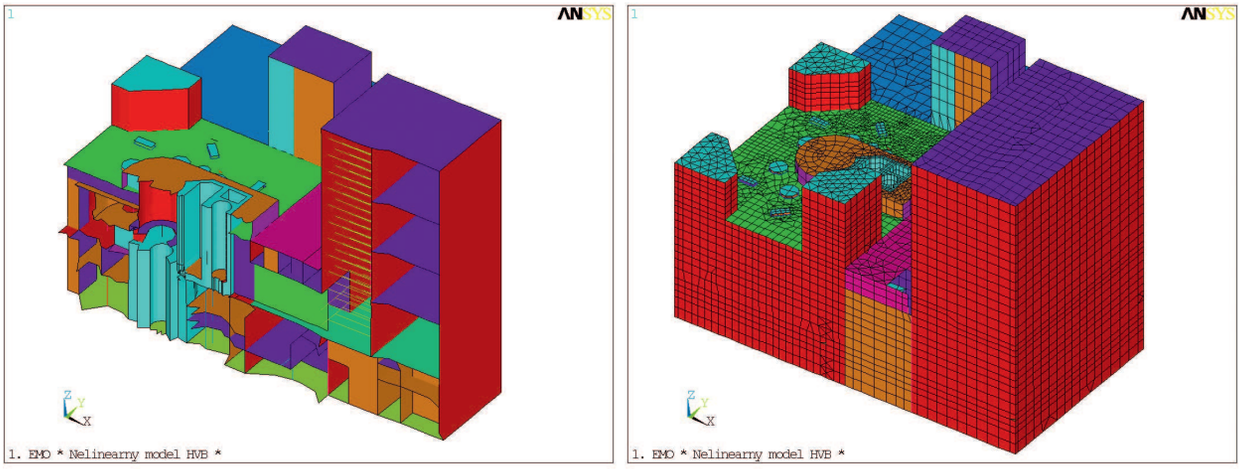


Figure 13. Calculation model of NPP VVER 440/213.

the critical area of hermetic zone failure. The cracking process started at the concrete slab along the middle wall due to concentration of the temperature and overpressure effects. There is the effective temperature gradient equal to 60–90°C in the middle plane of the wall and the plate. The mean value of the critical overpressure was equal to 352.5 kPa, and the max. strain is lower than 0.002 in the middle plane of the reinforced concrete panel.

The cracking process ($\varepsilon_1 \geq \varepsilon_t \doteq 0.0001$) at the bottom or top section of the reinforced concrete panels started when the overpressure was equal to 250 kPa.

The interior structures of the hermetic zone are loaded with the accident temperature equal to 150°C and the outside structures in the contact with the exterior are loaded by −28°C. The difference between the interior end of the exterior temperatures has significant influences to the peak strain in the structures.

The comparison of the strain shape from the linear and nonlinear solutions is presented in **Figure 14** and the stress shape in **Figure 15**. The strain increases and the stress decreases in the nonlinear solution in comparison with the linear solution.

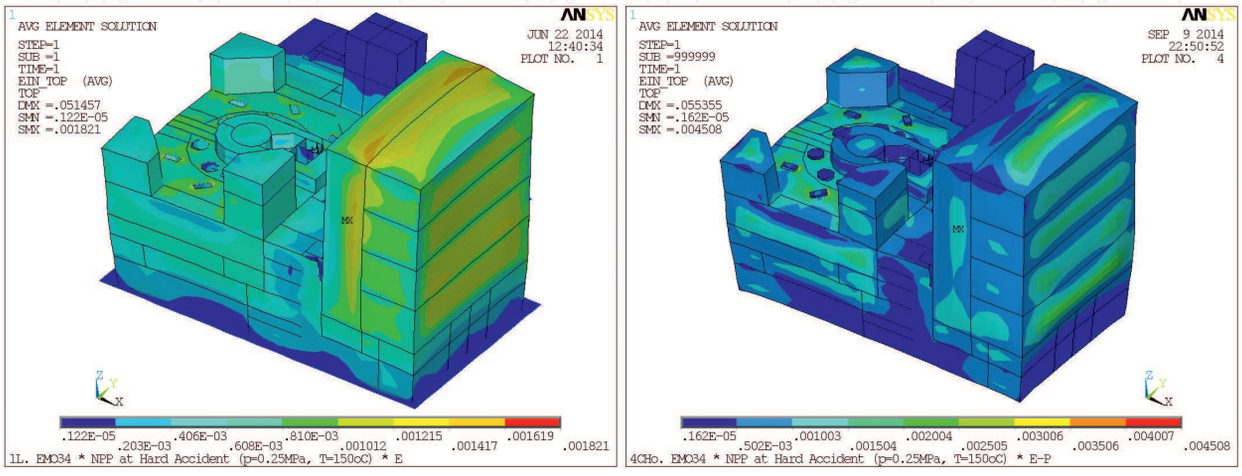


Figure 14. Strain intensity from the linear and nonlinear analysis.

http://dx.doi.org/10.5772/intechopen.68772

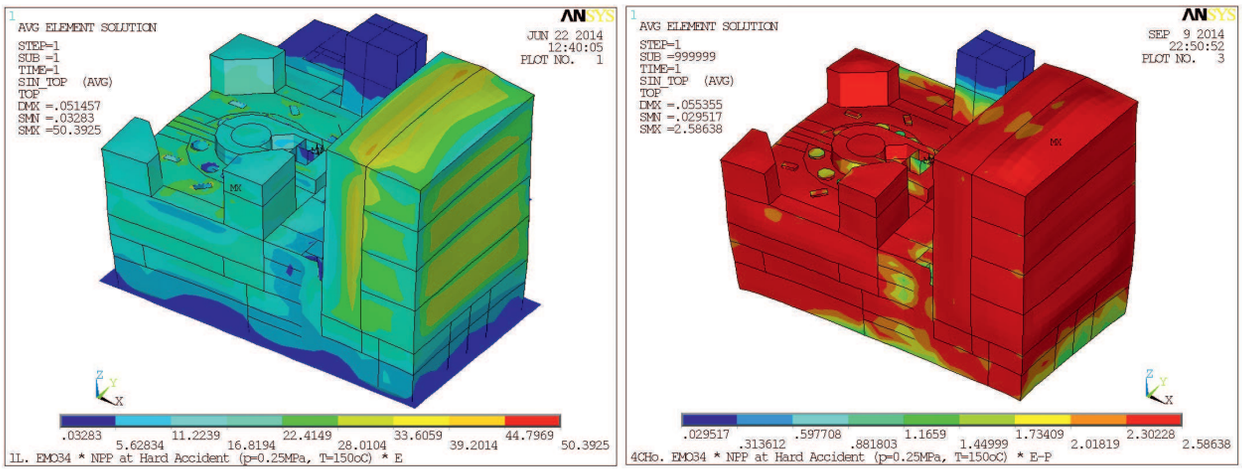


Figure 15. Stress intensity from the linear and nonlinear analysis.

5.2. Evaluation of the fragility curve

The probability of the containment failure was determined for this critical structure on the basis of the nonlinear deterministic analysis of the containment for various levels of the overpressure. The function of the failure was considered by Eqs. (28) and (29) for 10^6 Monte Carlo simulations in program FReET [32]. The probability of containment failure (**Figure 16**) is calculated from the probability of the reliability function RF in the form

$$P_f = P(RF < 0) \text{ and } RF = 1 - F_u(I_{\varepsilon 1}; J_{\varepsilon 2}; \varepsilon_u)/\varepsilon_u, \tag{35}$$

where the reliability condition RF is defined depending on a concrete failure condition (30).

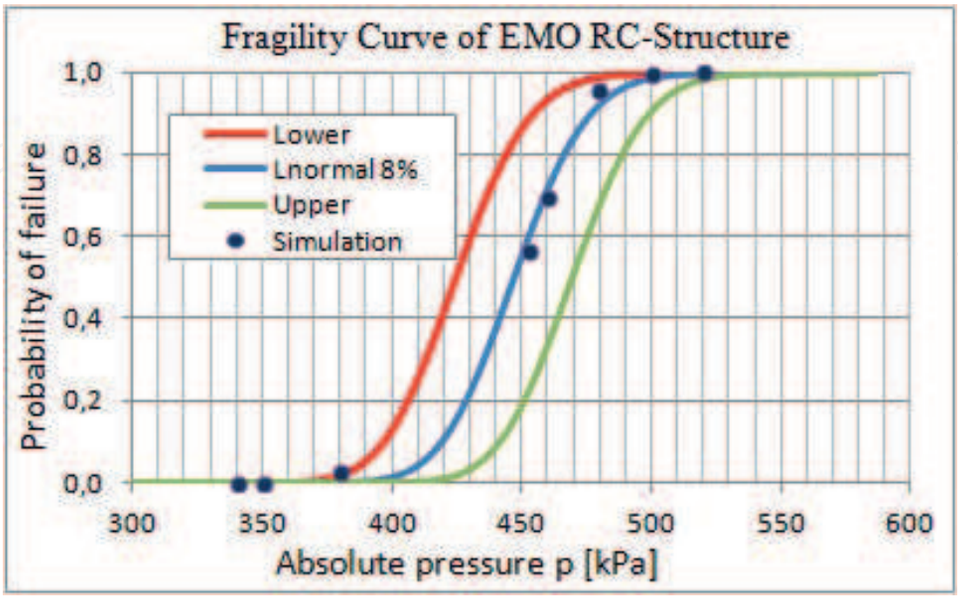


Figure 16. Fragility curve of failure pressure in the critical area of the hermetic zone under the accidental internal temperature $T_i = 150°C$ and external temperature $T_e = -28°C$.

6. Probabilistic analysis of the steel technology segments

The reactor and the bubble condenser-reinforced structures with steel liner represent the critical structures of the NPP hermetic zone [3]. Among the critical technology structures, the reactor hermetic covers and the reactor-protective hood, belong too [39, 40].

The reactor-protective hood is shown in **Figure 17**. The protective hood is an all-welded structure consisting of a spherical and a cylindrical part. The spherical part has a manhole of 500 mm in diameter with a ladder. The manhole facilitates equipment maintenance in the concrete cavity without the necessity to remove the protective hood. In order to ensure higher strength of the structure (on a seismic event), the protective hood is reinforced with a pipe (inner Ø712 mm) and six ribs. At the top, the pipe is welded in the canter of the hood spherical part, while the other end covers the ring on the upper block beam. The protective hood is set on a counter-flange and is attached to it with 60 M48 bolts and sealed with packing. The cap structure includes a platform with railing.

The finite element model of reactor cover was created in software ANSYS by the shell, beam, combine and mass elements. The envelope of cover is from layered shell elements (SHELL181). The surface load is defined using three-dimensional (3D) structural surface elements (SURF154). The connection with bolts is modelled by the combine elements (COMBINE14). The element of point mass (MASS21) represents the concentrated masses adequate to local load of the technology, beam elements (BEAM44) for frame and beam connection. The contact element (CE) and links (CP) were used for the joint connection. The upper part of the hood has

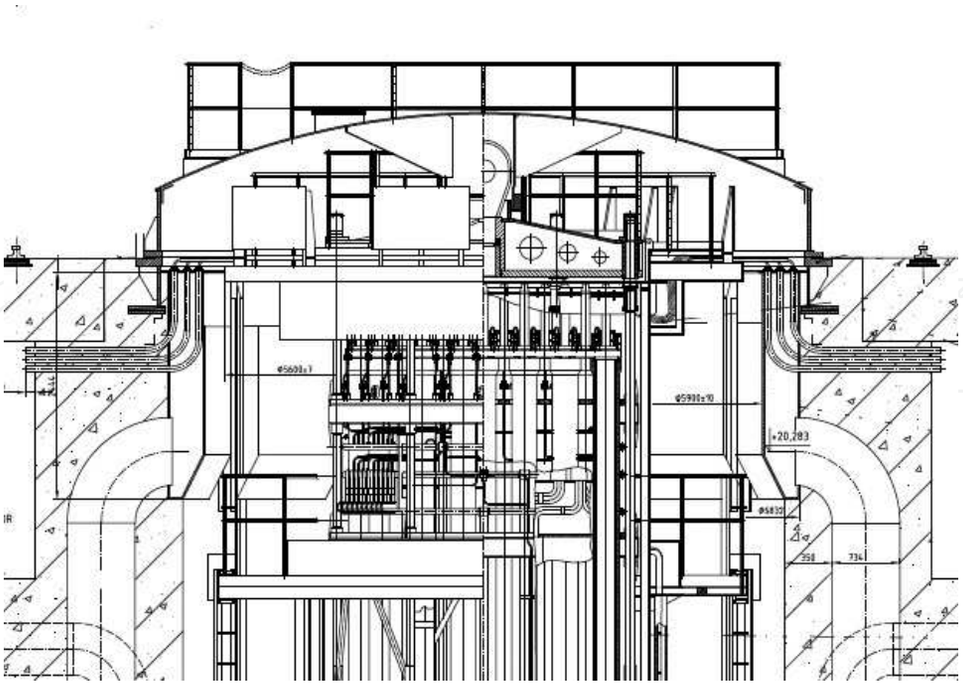


Figure 17. Vertical section of the reactor with reactor-protective hood.

http://dx.doi.org/10.5772/intechopen.68772

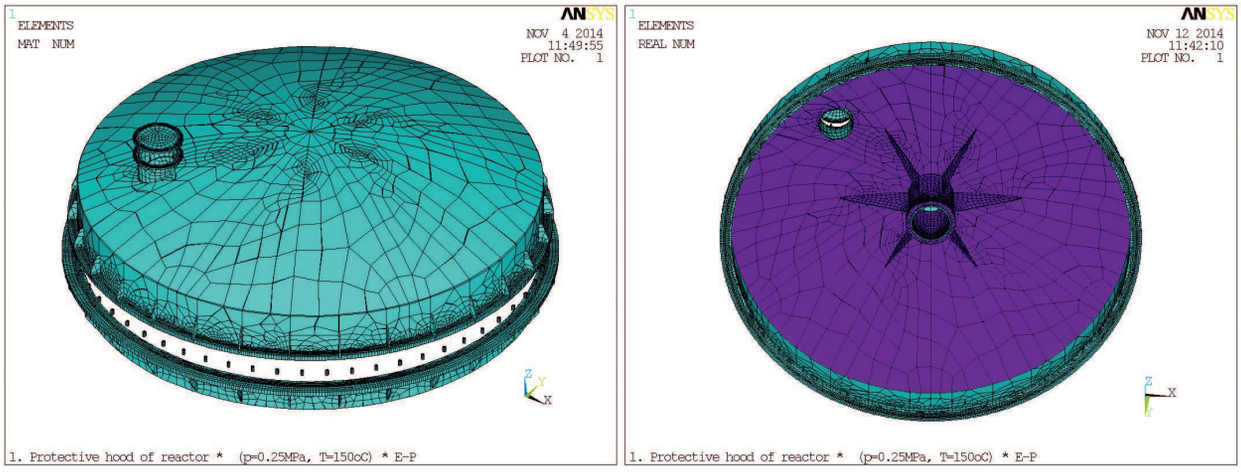


Figure 18. FEM model (RCOV) of the reactor-protective hood.

lugs used to handle it. The FEM model (RCOV) consists of 27,824 shell, beam and mass elements with 22,887 nodes (**Figure 18**).

6.1. Probability and sensitivity nonlinear analysis

The calculation of the probability of the reactor cover failure is based on the results of the nonlinear analysis for various levels of the accident pressure and mean values of the material properties. The critical areas of the technology segments defined from the nonlinear deterministic analysis are the mechanical closures. The CCD method of the RSM approximation is based on 45 nonlinear simulations depending on the six variable input data. The nonlinear solution for a single simulation consists of about 50–150 iterations depending on the scope of the plastic deformations in the calculated structures. The sensitivity analysis gives us the information about the influences of the variable properties of the input data on the output data (see **Figures 19** and **20**). These analyses are based on the correlation matrixes.

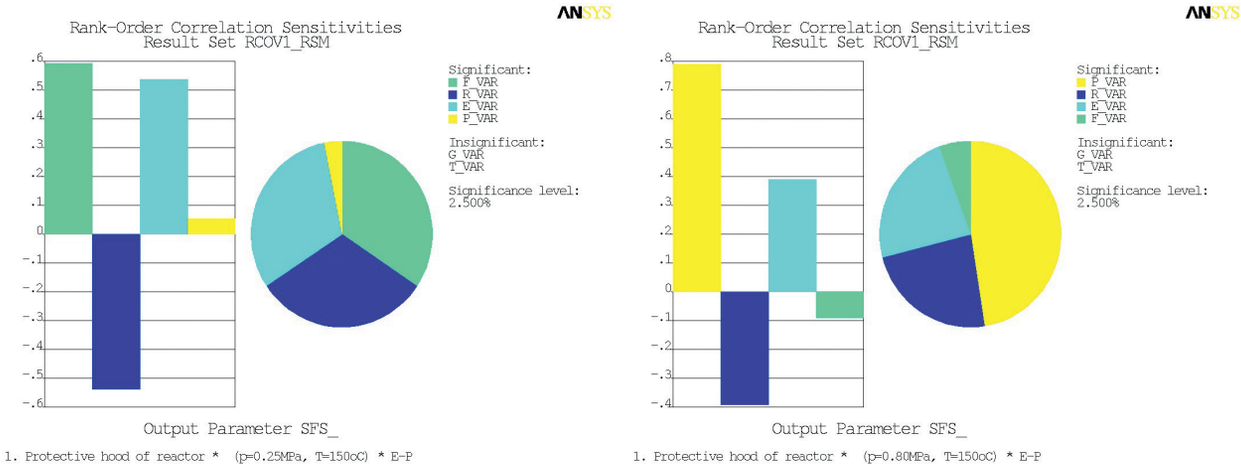


Figure 19. Sensitivity analysis of the safety function of the reactor-protective hood for overpressure Δp = 0.25 MPa and Δp = 0.80 MPa.

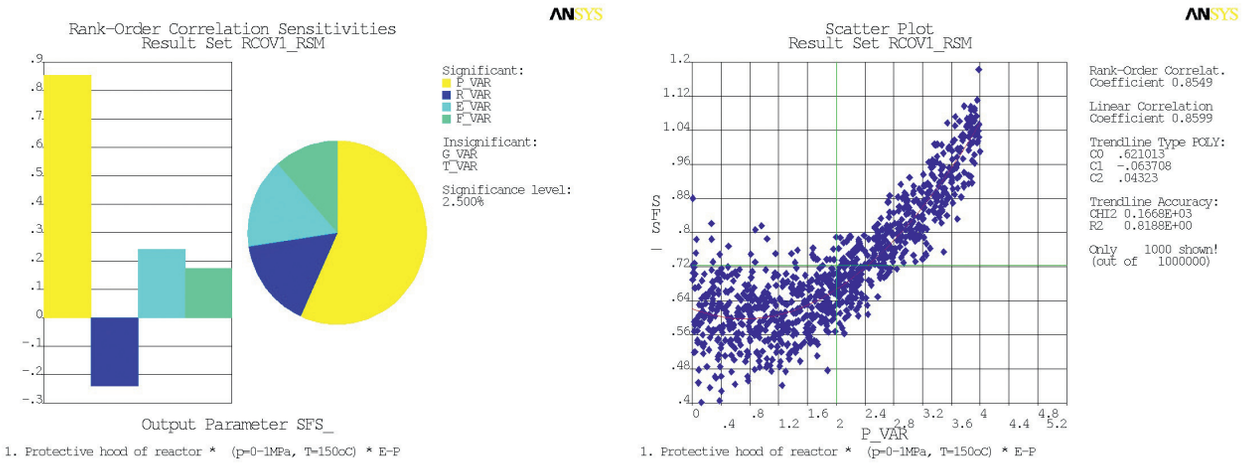


Figure 20. Sensitivity and trend analysis of the safety function of the reactor cover for uniform distribution of overpressure.

6.2. Fragility curves of failure pressure

The fragility curve of the failure pressure (see **Figure 21**) was determined performing 45 probabilistic simulations using the RSM approximation method with the experimental design CCD for 10^6 Monte Carlo simulations for each model and five levels of the overpressure. Various probabilistic calculations for five constant levels of overpressure next for the variable overpressure for gauss and uniform distribution were taken out. The nonlinear analysis of the steel technology structures was performed considering HMH-plastic criterion with the multilinear kinematic hardening stress-strain relations for various levels of the temperatures and the degradation of the strength. The uncertainties of the input data (**Table 3**) were

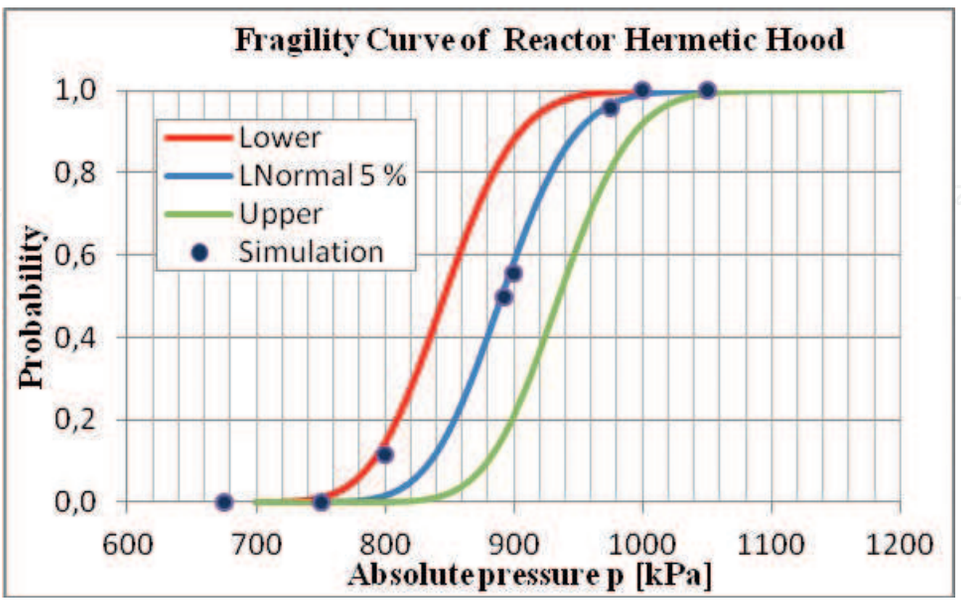


Figure 21. Fragility curves of the reactor-protective hood determined analytically for normal distribution with 5% envelope.

considered in accordance with the JCSS standards [30], NRC [11] and IAEA requirements [9]. The geometric and material nonlinearities of the steel solid and shell-layered elements were considered for the overpressure static loads from 250 to 1000 kPa.

7. Conclusions

The probability nonlinear analysis of the concrete containment failure was made for the overpressure loads from 250 to 500 kPa using the nonlinear solution of the reinforced concrete shell-layered elements. The CRACK program, which was developed by the author and implemented into the ANSYS system [3, 14–18], was used to perform the nonlinear analyses. The uncertainties of the load levels (temperature, dead and live loads), the material model of the composite structure (concrete cracking and crushing), reinforcement, and liner as well as other influences following from the inaccuracy of the calculated model and the numerical methods were taken into account in the Monte Carlo simulations [3]. The probability of the loss of the concrete containment integrity is less than 10^{-6} for the original structural model. The containment failure is equal to 0.050422906 for the overpressure of 275.5 kPa. The critical technology segment of the containment is the reactor-protective hood with the failure pressure $p_{u.0.05}$ = 766.9 kPa. The mean value of pressure capacity of the reactor-protective hood is $p_{u.0.50}$ = 891.8 kPa, the 95% upper bound is $p_{u.0.95}$ = 973.6 kPa.

Acknowledgements

The project was performed with the financial support of the Grant Agency of the Slovak Republic (VEGA 1/0265/16) and the Slovak Republic within the Research and Development Operational Programme for the project ‘University Science Park of STU Bratislava’, ITMS 26240220084.

Author details

Juraj Králik

Address all correspondence to: juraj.kralik@stuba.sk

Faculty of Civil Engineering, Slovak University of Technology in Bratislava, Bratislava, Slovakia

References

[1] HSG26. Safety Assessment Principles for Nuclear Facilities. 0 ed. http://www.onr.org.uk/saps/. Office for Nuclear Regulation; 2014. p. 226. ISBN: 978 0 7176 6456 6

[2] Pioro I. Handbook of Generation IV Nuclear Reactors. 1st ed. www.elsevier.com/books/handbook-of-generation-iv-nuclear-reactors/pioro. Woodhead Publishing; 2016. p. 940. ISBN: 9780081001622

[3] Králik J. Safety and Reliability of Nuclear Power Buildings in Slovakia. Earthquake-Impact-Explosion. 1st ed. www.martinus.sk/?uItem=103269. Bratislava: STU Bratislava; 2009. p. 307. ISBN: 978-80-227-3112-6

[4] NUREG/CR-1150. Severe Accident Risks, An Assessment for Five US Nuclear Power Plants, Summary Report, Final Summary Report. 1st ed. www.nrc.gov/reading-rm/doc-collections/nuregs/staff/sr1150/v1/. U.S. NRC; 1990. p. 59

[5] ENSREG. Stress Tests Performed on European Nuclear Power Plants, Post Fukushima Accident. 1st ed. www.oecd.nea.org/nsd/fukushima/documents. Brussels: European Commission Brussels; 2012. p. 53. DOI: v12i-2012-04-25

[6] NEA/CNRA/R12. Proceedings of the Forum on the Fukushima Accident: Insights and Approaches. 1st ed. www.oecd-nea.org/nsd/docs/2011/cnra-r2011-12.pdf. OECD; 2011. p. 127. DOI: JT03312480

[7] NRA SR. The Stress Tests for Nuclear Power Plants in Slovakia. 1st ed. www.ujd.gov.sk/files/NS_Zatazove_testy_JE_SR_ang.pdf. UJD SR; 2011. p. 186

[8] IAEA, Safety Standards No. SSR-2/1, Safety of Nuclear Power Plants: Design, Specific Safety Requirements. 1st ed. www/.iaea.org/books. Vienna: IAEA Vienna; 2012. p. 91. ISSN 1020–525X

[9] IAEA. Safety Series No. SSG-4, Development and Application of Level 2 Probabilistic Safety Assessment for Nuclear Power Plants. www-pub.iaea.org/books/iaeabooks/8236/Development-and-Application-of-Level-2-Probabilistic-Safety-Assessment-for-Nuclear-Power-Plants-Specific-Safety-Guide. IAEA; 2010. p. 88. ISBN: 978-92-0-102210-3

[10] IAEA TECDOC No. 1791. Considerations on the Application of the IAEA Safety Requirements for the Design of Nuclear Power Plants. www-pub.iaea.org/books/iaeabooks/11069/Considerations-on-the-Application-of-the-IAEA-Safety-Requirements-for-the-Design-of-Nuclear-Power-Plants. Vienna: IAEA Vienna; 2016. p. 84. ISBN: 978-92-0-104116-6

[11] NRC, RG 1.200. An Approach for Determining the Technical Adequacy of Probabilistic Risk Assessment Results for Risk-Informed Activities. www.nrc.gov/docs/ML0904/ML090410014.pdf. Washington, DC: U.S. Nuclear Regulatory Commission; 2009

[12] NUREG/CR-6813. Issues and Recommendations for Advancement of PRA Technology In Risk-Informed Decision Making. www.nrc.gov/reading-rm/doc-collections/nuregs/contract/cr6813/. Washington, DC: U.S. NRC Washington; 2003. p. 60. DOI: NRC Job Code B1564

[13] Kim DH, Ahn KI. Comparison of Nuclear Power Plant Risk using Dose-Based Risk Measure, Nuclear Science and Technology. Vol. 1. 2011 . pp. 440–443. DOI: 10.15669/pnst.1.440

[14] Králik J. A RSM method for probabilistic nonlinear analysis of reinforced concrete bubbler tower structure integrity. In: Proceedings of European Safety and Reliability Conference, ESREL 2009, (Eds); 7–10 September, Vol. 2; Taylor & Francis Group, Prague, CR; 2009. pp. 1369–1372. ISBN: 978-0-415-55509-8

[15] Králik J. Probabilistic safety analysis of the nuclear power plants in Slovakia. Journal of KONBiN, Safety and Reliability Systems. 2010;**2,3 (14, 15)** (VERSITA Central European Science Publishers):35–48. ISSN 1895–8281

[16] Králik J, Králik J, Jr. Probabilistic nonlinear analysis of bubble tower structure due to extreme pressure and temperature. In: Applied Mechanics and Materials: Selected, Peer Reviewed Papers from the Engineering Mechanics 2015; May 2015, Vol. 821; Svratka, CR; 2016. 725–732. ISSN 1660–9336.

[17] Králik J et al. Structural reliability for containment of VVER 440/213 type. In: Nowakowski et al., editors. Safety and Reliability: Methodology and Applications. Taylor & Francis Group, London; 2015. pp. 2279–2286. ISBN: 978-1-138-02681-0

[18] Králik J. Experimental and numerical analysis of the hermetic tightness of NPP bubble tower structure. In: Proceedings of the 3rd International Scientific Conference, Structural and Physical Aspects of Construction Engineering, SPACE 2016; November 2016; High Tatras. ISBN: 978-80-553-2643-6.

[19] Králik J. Probabilistic nonlinear analysis of the hermetic circular cover of main coolant pump failure due to extreme pressure and temperature. In: 22nd International Conference on Engineering Mechanics 2016; May 2016; Svratka, CR, ITAM AS Prague; pp. 309–312. ISSN 1805–8248

[20] Králik J. Probabilistic nonlinear analysis of NPP hermetic cover failure, due to extreme pressure and temperature. In: Transactions of the VSB, Civil Engineering Series, No. 2, June 2015, Vol. 15, TU Ostrava; 2015. p. 14. DE GRUYTER OPEN ISSN 1804–4824.

[21] HANDBOOK 3. Implementation of Eurocodes, Action Effects for Buildings, Development of Skills Facilitating Implementation of Eurocodes. Leonardo Da Vinci Pilot Project CZ/02/B/F/PP-134007; Aachen, 10.2005

[22] HANDBOOK 5. Implementation of Eurocodes Reliability Backgrounds. Design of Buildings for the Fire Situation. Development of Skills Facilitating Implementation of Eurocodes. Leonardo Da Vinci Pilot Project CZ/02/B/F/PP-134007; Aachen; 2005

[23] NUREG/CR-7031. A Compilation of Elevated Temperature Concrete Material Property Data and Information for Use in Assessments of Nuclear Power Plant Reinforced Concrete Structures; ORNL/TM-2009/175. US NRC; 2010

[24] ACI 349–90. Code Requirements for Nuclear Safety Related Concrete Structures. Detroit: American Concrete Institute; 1990

[25] CEB-FIP Model Code. Design Code. Thomas Telford; 1990. ISBN: 0727716964

[26] Kohnke P. ANSYS, Theory. Canonsburg: SAS IP Inc.; 2008. www.ansys.com

[27] Kolmar W. Beschreibung der Kraftuebertragung ueber Risse in nichtlinearen Finite-Element-Berechnungen von Stahlbeton-tragwerken [PhD thesis]. Darmstadt: T.H. Darmstadt; 1986

[28] Jerga J, Križma M. Assessment of Concrete Damage, Building Research Journal 54. 2006. pp. 79–100. DE GRUYTER, ISSN 1339-682X

[29] Haldar A, Mahadevan S. Probability, Reliability and Statistical Methods in Engineering Design. New York, NY: John Wiley & Sons; 2000. https://www.amazon.com/Probability-Reliability-Statistical-Methods-Engineering/dp/0471331198

[30] JCSS 2011. JCSS Probabilistic Model Code. Zurich: Joint Committee on Structural Safety. <www.jcss.byg.dtu.dk>

[31] Bažant ZP, Pang SD, Vořechovský M, Novák D. Energetic-statistical size effect simulated by SFEM with stratified sampling and crack band model. International Journal for Numerical Methods in Engineering (Wiley). 2007;**71**(11):1297–1320. [Rep. Dept. of Civil Eng., Northwestern University, Evanston, Illinois]

[32] Novák D, Bergmeister K, Pukl R, Červenka V. Structural assessment and reliability analysis for existing engineering structures, Theoretical background. Structure and Infrastructure Engineering. 2009;**9**(2):267–275

[33] Melcher J, Kala Z, Holický M, Fajkus M, Rozlívka L. Design characteristics of structural steels based on statistical analysis of metallurgical products. Journal of Constructional Steel Research. 2004;60(3–5):795–808

[34] Kala Z, Melcher J, Puklický L. Material and geometrical characteristics of structural steels based on statistical analysis of metallurgical products. Journal of Civil Engineering and Management. 2009;**15**(3):299–307

[35] Krejsa M, Králik J. Probabilistic computational methods in structural failure analysis. Journal of Multiscale Modelling. 2015;**6**(2)p. 5. Imperial College Press, DOI: 10.1142/S1756973715500067

[36] Suchardová P, Bernatík A, Sucharda O. Assessment of loss results by means of multi - Criteria analysis. In: Advances in Safety, Reliability and Risk Management, Proceedings of the European Safety and Reliability Conference, ESREL 2011; London: CRC Press-Taylor & Francis Group; 2011. pp. 1563–1570. ISBN: 978-0-415-68379-1

[37] Sýkora M, Holický M. Assessment of Uncertainties in Mechanical Models, Applied Mechanics and Materials. Vol. 378. Switzerland: Trans Tech Publications; 2013. pp 13–18. doi:10.4028/www.scientific.net/AMM.378.13

[38] Vejvoda S, Keršner Z, Novák D, Teplý B. Probabilistic safety assessment of the steam generator cover. In: Proceedings of the 17th International Conference on Structural Mechanics in Reactor Technology (SMiRT 17); 2003 August 17–22; Prague, CR; M04-4; 2003. p. 10. https://www.iasmirt.org/smirt/17/transactions

[39] Králik J. Probabilistic nonlinear analysis of the hermetic circular cover of main coolant pump failure due to extreme pressure and temperature. In: 22nd International Conference on Engineering Mechanics 2016, Vol. 821; May 2016; Svratka, CR; 2016. pp. 309–312. ISSN 1805–8248

[40] Králik J. Probabilistic nonlinear analysis of NPP hermetic cover failure due to extreme pressure and temperature. In: Transactions of the VSB, Civil Engineering Series, No. 2, June 2017, Vol. 15, No. 2; TU Ostrava; 2017. p. 14. DE GRUYTER OPEN, ISSN 1804-4824

IntechOpen

IntechOpen

IntechOpen